Application of Power Spectrum, Cepstrum and Higher Order Spectrum and Neural Network Analyses for Induction Motor Fault Diagnosis

B.Liang, S.D.Iwnicki and Y.Zhao

Faculty of Computing and Engineering, Huddersfield University, UK
B.liang@hud.ac.uk

Abstract

The power spectrum is defined as the square of the magnitude of the Fourier transform (FT) of a signal. The advantage of FT analysis is that it allows the decomposition of a signal into individual periodic frequency components and establishes the relative intensity of each component. It is the most commonly used signal processing technique today. If the same principle is applied for the detection of periodicity components in a Fourier spectrum, the process is called the cepstrum analysis. Cepstrum analysis is a very useful tool for detection families of harmonics with uniform spacing or the families of sidebands commonly found in gearbox, bearing and engine vibration fault spectra. Higher order spectra (HOS) (also known as polyspectra) consist of higher order moment of spectra which are able to detect non-linear interactions between frequency components. For HOS, the most common used is the bisoectrum. The bispectrum is the third-order frequency domain measure, which contains information that standard power spectral analysis techniques cannot provide. It is well known that neural networks can represent complex non-linear relationships, and therefore they are extremely useful for fault identification and classification. This paper presents an application of power spectrum, cepstrum, bispectrum and neural network for fault pattern extraction of induction motors. The potential for using the power spectrum, cetstrum, bispectrum and neural network as means for differentiating between healthy and faulty induction motor operation is examined. A series of experiments are done and the advantages and disadvantages between them are discussed.

Keywords

Induction motors, vibration, fault pattern identification, power spectrum, cepstrum, bispectrum, signal processing

1. INTRODUCTION

Vibration and phase current analysis are widely used in condition monitoring and fault diagnosis of induction motors. Since variations of vibration and phase current contain valuable information about the condition of the machine. By analysing the signals people can in many cases predict whether a machine is about to develop a fault. Generally speaking the vibration signals picked up by an accelerometer and the phase current signals picked up by a Hall-effect sensor have to be processed in some way. The raw vibration and phase current signals are rarely used in practice. For example, the overall mean square value, variance value, skewness, kurtosis of a signal are likely to be used in time domain, while in frequency domain the Fourier analysis of a signal like the power spectrum (the second-order frequency domain measure) is commonly used. Although the power spectrum has been widely used in various fields like vibration, acoustic, radar, sonar, telecommunication and image processing, one of its inherited drawbacks is that it will lose the phase information between frequency components. Recently, more elaborate procedures are being studied, such as higher-order spectrum analysis [1]. The motivations behind the use of higher order spectrum analysis are as follows [2]. Firstly, the technique can suppress Gaussian noise processes of unknown spectral characteristics in detection, parameter estimation and classification problems. If a non-Gaussian signal is embedded in additive Gaussian noise, a transform to HOS will eliminate the noise. The non-Gaussianess condition is satisfied in many practical applications, since any periodic or quasi-periodic signals can be regarded as a non-Gaussian signal, and self-emitting signals from complicated machinery can also be considered as non-Gaussian signals. Secondly, HOS preserves the phase information. For example, there are situations in practice in which the interaction between two harmonic components causes contribution to the power at their sum and/or difference frequencies. Thirdly, HOS can play a key role in detecting and characterising the type of non-linearity in a system from its output data. Although HOS has been developed as a signal processing tool over a period of 30 years it has been mostly used to speech signal processing and sonar signal processing. The application of HOS for condition monitoring and fault diagnosis of machinery is relatively seldom found. In [3-4] some excellent work has been done by Gu and Ball, however, they have concentrated on the application of HOS in electrical motor current analysis. Another approved useful method adopted by this paper for complicated multiband frequency analysis is the cepstrum analysis which is considered as the spectrum analysis of the logarithm spectrum of a signal. The cepstrum can be seen as information about the rate of change in the different spectrum bands. Despite it has found widely applications in engine gearbox and bearing condition monitoring and fault diagnosis [5-6], the application for

induction motor fault diagnosis has not been reported yet. In the condition monitoring and diagnostics of machinery, two fundamental problems exist, namely, (1) the identification and classification of fault patterns; and (2) the quantification of fault development. Mathematically, the former is a clustering problem and the latter is a trend analysis problem. Fault identification and classification involves the processing of a large amount of information contained in the monitored signals. Inevitably there exist some uncertainties and non-linearity in machinery due to system complexity and measurement errors. Neural networks represent one of the distinct methodologies that deal with uncertainty. Neural networks can represent complex non-linear relationships, and they are very good at classification of phenomena into pre-selected categories as used in the training process. Hence, they can be particularly useful for the problems of condition monitoring and diagnostics. This paper presents an investigation of power spectrum, cepstrum, higher order spectrum and neural network analysis for induction motor condition monitoring and fault diagnosis. For HOS the investigation is mainly concentrated on the bispectrum analysis (the third-order frequency domain measure) of vibration and phase current signals. The paper is organised as follows: the section 2 introduces the basic theory of the power spectrum, cepstrum and bispectrum. In the section 3 the fundamental fault theory for induction motors are presented. The experimental results and analysis are shown in section 4. Finally the conclusions are given.

2 THE BASIC THEORY OF POWER SPECTRUM, CEPSTRUM AND HIGH ORDER SPECTRUM

2.1 Power spectrum definition

The power spectrum is defined as the square of the magnitude of the FT of a signal. It can be written as:

$$P(\omega) = \left| \int_{-\infty}^{+\infty} x(t) e^{-j\omega t} \right|^2 = X(\omega) \cdot X^*(\omega) \tag{1}$$

Where $X(\omega) = \int_{-\infty}^{+\infty} x(t) e^{-j\omega t} dt$ is the FT of a signal and $X^*(\omega)$ is its complex conjugate, and $\omega = 2\pi f$, f is frequency in Hz.

2.2 Cepstrum definition

A cepstrum is usually defined as the Fourier transform of the logarithm of the Fourier transform of a signal. The name of cepstrum was deprived by reversing the first four letters of spectrum. There is a real cepstrum, a complex cepstrum, a power cepstrum and a phase cepstrum.

The real cepstrum of a signal x(t) $$c(t) = \frac{1}{2\pi} \int_{-\pi}^{\pi} \ln|X(\omega)| e^{j\omega t} d\omega \tag{2}$$

The complex cesptrum of a signal $$\hat{c}(t) = \frac{1}{2\pi} \int_{-\pi}^{\pi} \ln X(\omega) e^{j\omega t} d\omega \tag{3}$$

The power cepstrum of a signal $$\tilde{c}(t) = \frac{1}{2\pi} \left| \int_{-\pi}^{\pi} \ln|X(\omega)|^2 e^{j\omega t} d\omega \right|^2 \tag{4}$$

The most commonly used cepstrum is the power cepstrum. The algorithum of power cepstrum of a signal can be summarized as: signal → FFT → abs() → square → log → FFT → abs() → square → power cepstrum.

2.3 Higher order spectrum definition

Although the mathematics is not central to the current investigation, a few explanations are necessary. It is well known that the first-order cumulant of a stationary process is the mean,

$$C_1 x := E\{x(n)\} \tag{5}$$

The second and third-order cumulants of a stationary process are defined by [5] as follows:

$$C_2 x(k) = E\{x^*(n)x(n+k)\} \tag{6}$$

$$C_3x(k,\,l) = E\{x^*(n)x(n+k)x(n+l)\} - C_2x(k)C_2x(l-m) - C_2x(l)C_2x(k-m) \quad (7)$$

Higher order spectra (also known as polyspectra), are defined as Fourier transform of the corresponding cumulant sequences. The conventional power spectrum is, in fact, the FT of the second-order cumulant. The third-order spectrum also called the bispectrum which is, by definition, the Fourier transform of the third-order cumulant. Figure 1 shows the higher order spectra classification of a given discrete time signal.

$$S_{2x}(\omega) = \sum_{k=-\infty}^{\infty} C_{2x}(k)e^{-j\omega k} \quad (8)$$

$$S_{3x}(\omega_1, \omega_2) = \sum_{k=-\infty}^{\infty} \sum_{l=-\infty}^{\infty} C_{3x}(k, l)e^{-j\omega_1 k}e^{-j\omega_2 l} \quad (5)$$

The corresponding relationships between high order cumulants and polyspectra are presented in Figure 1.

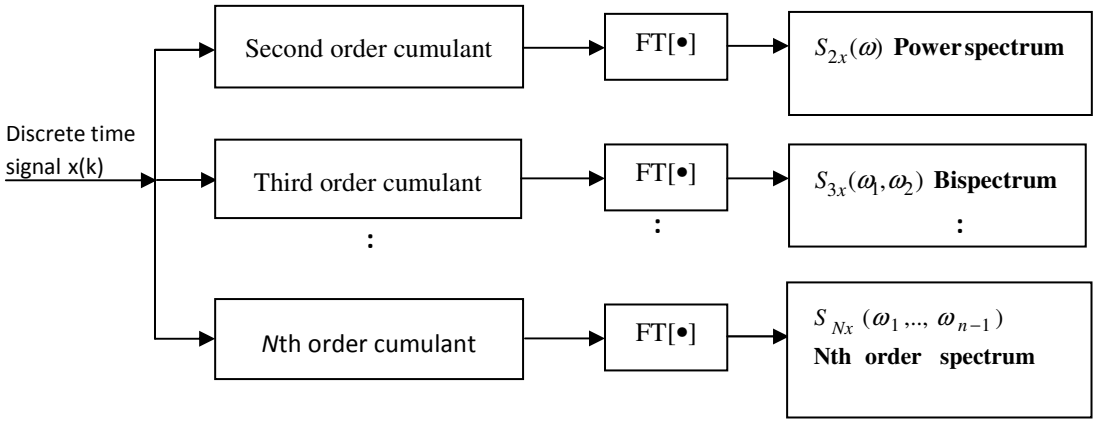

Figure 1 The relationship between higher order cumulants and polyspectra

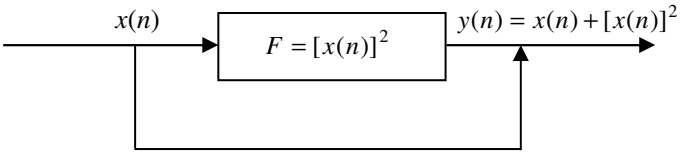

Figure 2 A simple generater for a QFC signal

Note that the bispectrum $S_{3x}(\omega_1,\omega_2)$ is a function of two frequencies. Therefore, it can detect phase coupling between two frequencies which appears as a third frequency at the sum or difference of the first two with a phase that is also the sum or difference of the first two. In order to illustrate this, Figure 2 presents a simple transfer function with square non-linear characteristics [7]. Supposing the input signal $x(n) = \sum_{k=1}^{2} \cos(2\pi f_k n + \alpha_k)$, then the output signal is:

$$y(n) = x(n) + [x(n)]^2 = \cos(2\pi f_1 n + \alpha_1) + \cos(2\pi f_2 n + \alpha_2) + \frac{1}{2}\cos(4\pi f_1 n + 2\alpha_1) + \cos\big(2\pi(f_1 + f_2)n + (\alpha_1 + \alpha_2)\big) + \cos\big(2\pi(f_1 - f_2)n + (\alpha_1 - \alpha_2)\big) + \frac{1}{2}\cos(4\pi f_2 n + 2\alpha_2) \quad (6)$$

Obviously, the output signal $y(n)$ is much richer in its component content than the input signal $x(n)$. It also shows that there are certain phase relations of the same type, such as the frequency relations (f_1,α_1), $(f_2,\alpha_2),(2f_1,2\alpha_1),(2f_2,2\alpha_2),(f_1+f_2,\alpha_1+\alpha_2)$ and $(f_1-f_2,\alpha_1-\alpha_2)$ This phenomenon is called quadratic phase coupling (QPC) [8-10]. Traditionally power spectrum is used to break down the signals into a series of frequency components. However, power spectrum cannot determine whether peaks at

harmonically related positions are phase coupled since the power spectrum uses only the magnitude of the Fourier components and phase information is neglected. Higher order spectral estimates like bispectrum use phase information and are capable of detecting phase coupling. Therefore the bispectrum can provide additional frequency information which the conventional power spectrum cannot give. It can be proved that the QPC characterization does exist in the following application of induction motor fault diagnosis. Due to the radial flux density waves between stators and rotors of induction motors the Maxwell tensile stresses are developed [11]. The tensile stress can be expressed in tensile force per unit surface area and is proportional to the square of the flux density. Equation (1) gives a general expression for the tensile stress $F(x,t)$:

$$F(x,t) = [B_f(x,t) + \sum_s B_s(x,t) + \sum_r B_r(x,t)]^2 / 2\mu_0 \quad (7)$$

Where $B_f(x,t)$ is the fundamental flux density that is the function of harmonics. The $\sum_s B_s(x,t)$ and $\sum_r B_r(x,t)$ are the stator and rotor harmonic flux densities, respectively. Clearly, $F(x,t)$ looks like the same form as the above QPC example in term of square components, therefore, the induction motor' radial vibration which is mainly caused by the tensile stress will have some QPC characteristics.

The advantages of using high order spectral analysis can be summarised as follows [12]:

(1) If the measurement *x(n)* is Gaussian, the cumulants $C_m x(n)=0$ for $m > 2$. It means it can be used to suppress Gaussian noise.
(2) If *x(n)* is symmetrically distributed, the $C_3 x(k,l)=0$. The third-order cumulant eliminates both Gaussian and symmetrically distributed processes.
(3) For cumulant additives, $x(n)=s(n)+w(n)$, where *s(n)* and *w(n)* are independent and *w(n)* is Gaussian stationary processes, then $C_m x(n)=C_m s(n)$ for $m > 2$. It indicates that high-order cumulants can provide us noise free signals if certain conditions are met.
(4) Extra QPC information is available.
(5)

The Third-Order Higher Spectral Algorithm (Bispectrum) Implementation.

There are many different algorithms for higher-order spectral estimation. The direct calculation algorithm was adopted as follows:

(1) Let $\boldsymbol{x}=[x_1,x_2,\ldots x_m]$ is the original data record, segment the data into *k* possibly overlay records.
(2) De-trend and remove the mean of each record.
(3) Add windows and compute the FFT of each record, based on *M* points (default 128 points).
(4) The bispectrum $\boldsymbol{B}_k$ of the *kth* order record is computed as $\boldsymbol{B}_k=\boldsymbol{X}_k(m)\boldsymbol{X}_k(n)\boldsymbol{X}_k^*(m+n)$, where $\boldsymbol{X}_k$ denotes the FFT of the *kth* record.
(5) Finally average and smooth the bispectrum across the records.

3. FAULT SYMTOM ANALYSIS FOR OF INDUCTION MOTORS

3.1 Induction motor fault symptom analysis

Induction motor is one most widely used driving powers in industry. A variety of faults can occur within induction motors like stator winding fault or broken rotor bar in rotor. In general, in a three-phase induction motor the windings of the individual phases are displaced 120-degrees from each other. Figure 4 illustrates a simplified two-pole three-phase stator winding. When three phase alternating currents are applied to the stator windings the following fundamental components of magneto-motive force (mmf) of three-phase windings are produced [13]

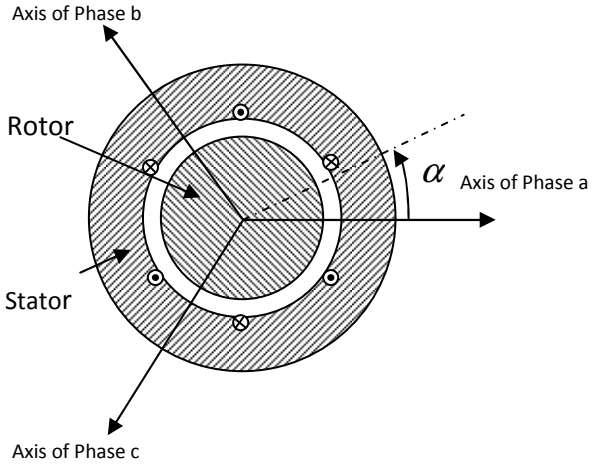

Figure 3 A simplified two-pole three-phase stator winding

$$
\begin{aligned}
F_a &= F_{\max}\cos\alpha\cos\omega t \\
F_b &= F_{\max}\cos(\alpha-\frac{4}{3}\pi)\cdot\cos(\omega t-\frac{4}{3}\pi) \\
F_c &= F_{\max}\cos(\alpha-\frac{4}{3}\pi)\cdot\cos(\omega t-\frac{4}{3}\pi)
\end{aligned}
\tag{11}
$$

Where $\omega = 2\pi f$, and f is the supply frequency

The three mmfs F_a , F_b and F_c can be individually divided into the positive sequence component (F_a^+ , F_b^+ , F_c^+) and the negative sequence component (F_a^- , F_b^- , F_c^-) as follows:

$$
\begin{aligned}
F_a &= \frac{1}{2}F_{\max}\cos(\alpha-\omega t)+\frac{1}{2}F_{\max}\cos(\alpha+\omega t) \Leftrightarrow F_a = F_a^+ + F_a^- \\
F_b &= \frac{1}{2}F_{\max}\cos(\alpha-\omega t+\frac{4}{3}\pi)+\frac{1}{2}F_{\max}\cos(\alpha+\omega t-\frac{4}{3}\pi) \Leftrightarrow F_b = F_b^+ + F_b^- \\
F_c &= \frac{1}{2}F_{\max}\cos(\alpha-\omega t+\frac{2}{3}\pi)+\frac{1}{2}F_{\max}\cos(\alpha+\omega t-\frac{2}{3}\pi) \Leftrightarrow F_c = F_c^+ + F_c^-
\end{aligned}
\tag{12}
$$

If the fundamental components of mmfs in a symmetrical three phase winding carrying a symmetrical set of currents are added together, it can be found that:

$$
\begin{aligned}
F^+ &= F_a^+ + F_b^+ + F_c^+ = 3F_a^+ \\
F^- &= F_a^- + F_b^- + F_c^- = 0
\end{aligned}
\tag{13}
$$

From this result it can be concluded that for symmetrical three-phase windings fed by a set of symmetrical currents, only positive sequence components of mmfs are left. Negative sequence components of mmfs are summed to zero. The symmetrical stator winding produces a rotating field at frequency f when supply currents are applied to the stator windings. This rotating field induces electromagnetic forces in the rotor bar at a frequency of sf (where s is the slip of the induction motor). Since the rotor bars with end ring can be viewed as rotor phase windings, the induced alternating currents will flow through the rotor bars. Then, the phase windings with the induced alternating currents of the rotor will also produce only a positive fundamental

component of mmf of the rotor, which rotates at frequency sf if the rotor is symmetrical. A broken rotor bar or some other fault condition within the rotor will create an asymmetry. The induced currents of the rotor will cause a negative sequence component in addition to a positive sequence component in the stator windings because the resultant negative sequence component is no zero any more. As the resultant negative component rotates at frequency $-s\omega$ (backward) with respect to the rotor, whereas the rotor rotates with frequency $(1-s)f$, the resultant negative consequence component will rotate forward with respect to the stator. It can be seen that the stator currents now consist of the normal supply frequency f, together with a component $(1-2s)f$. The variable frequency component has the effect of modulating the power supply frequency component at twice slip frequency. This can be reflected in the stator-winding conductors and therefore appears in the supply currents as a modulation of the supply frequency at $(1\pm 2s)f$. The upper side band is due to the speed variation resulting from the lower side band current. Due to the change in the flux density, the stator core vibration will also be modulated at $\pm 2sf$ frequencies around the motor speed and the rotor slot harmonics, since magnetic forces are proportional to the flux density waveform squared. It is also well known that the side band frequencies appear around the fifth, seventh and higher order harmonics [14-15] when there is a broken rotor bar. These symptom frequencies can be given by the following formula:

$$f_{asymmetric} = 2\pi f[k(1-s)/p \pm s],\ k=1,2,3,\ldots \tag{14}$$

Similarly if there is an asymmetry in stator caused by winding shortcut or unbalances three phase power supply, the negative sequence components of mmfs are not summed zero as well. It will create an extra stator and rotor current which produces an unwanted pulsing torque in the induction motor as indicated below [16].

$$T_{pulsating} = (3P/2\pi f)\,\mathrm{Re}[(\bar{V}_{s1}\bar{I}_{s2} - \bar{V}_{s2}\bar{I}_{s1})e^{j2\omega t}] \tag{15}$$

Where $\bar{V}_{s1}, \bar{V}_{s2}$ and $\bar{I}_{s1}, \bar{I}_{s2}$ are the positive and negative consequence components of stator voltage and current. P is the pole pairs of induction motor. It can be seen that this is a torque component which pulsating at the angular frequency $2\pi f = 2\omega$. The pulsating torque is caused by the interaction of the positive sequence stator current and negative sequence stator flux linkages and also by the interaction of the negative sequence stator currents and positive sequence stator flux linkages respectively. Therefore, the 2ω double frequency time varying pulsating torque component can be used as the faulty symptom of the asymmetrical stator system.

3.2 Experimental test rig

In order to test the proposed high order spectrum and cepstrum methods for condition monitoring and fault diagnosis of induction motors, a series of experiments were carried out on an induction motor test rig. The basic test rig is shown in Figure 3. It consists of a 3kW, 4-pole, rated speed 1450rpm AC induction motor with a 5 kW DC motor used to absorb the generated power. Five accelerometers were attached at two ends of the induction motor to measure vibration of the induction motor and three phase current sensors were used to measure induction motor currents. A speed encoder with 3600 pulse per revolution was installed to measure the instantaneous speed of the induction motor. The general basis for induction motor fault detection is that a fault in the motor circuit causes an asymmetry in the flux density across the motor circuit and this flux imbalance rotates with the rotor. The effect of this rotating electrical imbalance can be detected both in stator vibration and consumed current and transient rotor speed, and in each case it appears as a modulation effect with a modulating frequency of twice slip. A series of test have been done and presented to show the load effect on the slip. In order to maximize the slip effect, all other experiments have been done under full load and the rated maximum speed around 1450 rpm. A few faults were created within the induction motor, such as broken rotor bar and asymmetrical stator system faults. The broken rotor bar fault was made with artificially cutting one rotor bar. The asymmetrical stator system was done by creating 20v and 40v voltage unbalances between 3-phase stator voltage supplies.

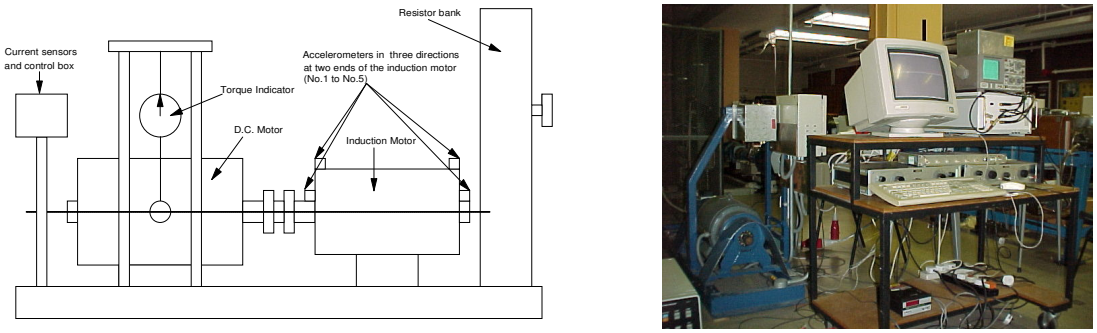

Figure 4 The induction motor test rig

From statistical theory it is known that the first order zero-lag cumulant is the mean, the second order zero-lag cumulant represents variance, the third order zero-lag cumulant represents skewness and fourth order zero-lag cumulant provides an indication of kurtosis. These parameters can be used to describe the statistical characteristic of a signal. Table 1 shows the average mean, variance, skewness and kurtosis of fifty vibration sample values for an induction motor under different fault conditions.

Table 1 - Average Values of Mean, Variance, Skewness and Kurtosis

	Normal Healthy Operation	**One Broken Rotor Bar**	**20V Drop in One Phase Supply**	**40V Drop in One Phase Supply**
Mean	0.0018	0.0020	0.0023	0.0026
Variance	0.0005	0.0026	0.0203	0.0305
Skewness	0.0247	0.0311	0.0588	0.0696
Kurtosis	1.8268	2.8346	3.01972	3.22367

The results show these parameters change with the occurrence of a fault condition. The variance values increase with the seeding of a broken rotor bar and then with 20V and 40V drops in one phase of supply. The kurtosis and skewness parameters also increase with the introduction of the faults. Although the statistical measures indicate the presence of a fault they do not provide any information for the type of that fault.

As indicated in section 3.1, some faulty symptoms are to identify the sidebands which are closely related with motor slip. Due to the fact slip are dependent on the motor load. Therefore the motor load has effects to identify the sidebands. Figures 5-7 present the vibration power spectra of induction motor with and without broken rotor bar fault under 0%, 50% and 100% motor load conditions. It can seen that there is no visible sidebands for broken rotor fault under 0% motor load since the slip is too small to be identified (figure 5). However clear sidebands are available for the same broken rotor bar fault under 50% motor load (figure 6). When the motor load is increased to 100% load, the sidebands around the rotor speed move further outward from the rotor speed (figure 7). The same phenomenon can be observed in the stator current power spectra of induction motor. Figures 8-10 show the stator current power spectra of induction motor under 0%, 50% and 100% motor load conditions. As shown in figure 8, no visible sidebands exist around the main power supply frequency 50 Hz. But for 50% motor load, the sidebands can be clearly identified in figure 9. For 100% motor load, the stator current spectrum of induction motor demonstrates the exact same characteristic as the vibration power spectrum of induction motor. The sidebands shift further away from the centre of main supply frequency 50 Hz in figure 10. Both vibration and stator current power spectra can identify broken rotor bar faults clearly provided a certain amount load is exerted on the motor. But, the stator current spectrum demonstrates slightly better performance than the vibration power spectrum in term of frequency line identification and tidiness of the spectrum.

The results for 20V and 40V drop in one phase supply of three-phase supply are given in figure 11-12. It demonstrates that there are obvious amplitude increasing at fault frequency 2ω=100Hz in both vibration and stator current spectra. This proved the previous theory analysis. It is also observed that there are rich frequency sidebands in the stator current spectra with 20V and 40V drop of one phase power supply.

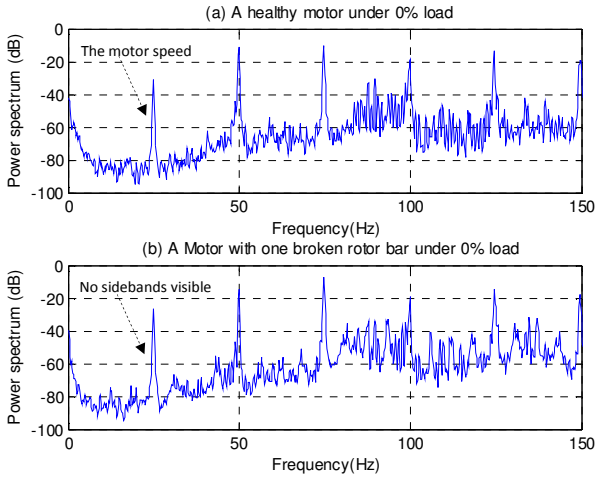

Figure 5 The vibration power spectra of induction motor without and with broken rotor bar fault under 0% load

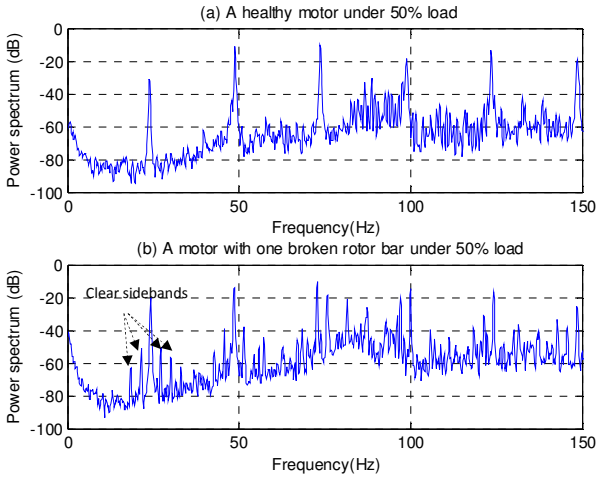

Figure 6 The vibration power spectra of induction motor without and with broken rotor bar fault under 50% load

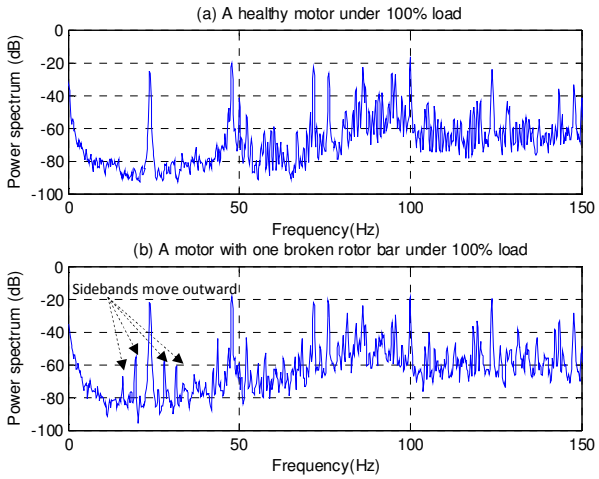

Figure 7 The vibration power spectra of induction motor without and with broken rotor bar fault under 100% load

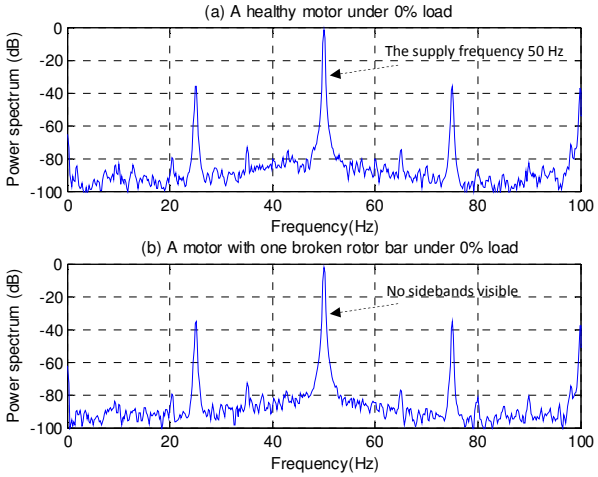

Figure 8 The stator current power spectra of induction motor without and with broken rotor bar fault under 0% load

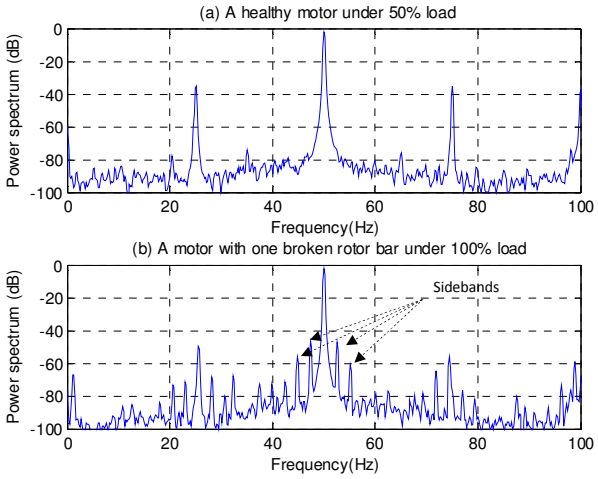

Figure 9 The stator current power spectra of induction motor without and with broken rotor bar fault under 50% load

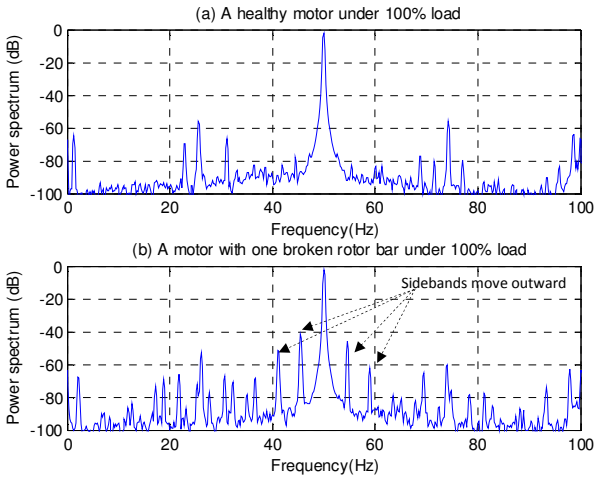

Figure 10 The stator current power spectra of induction motor without and with broken rotor bar fault under 100% load

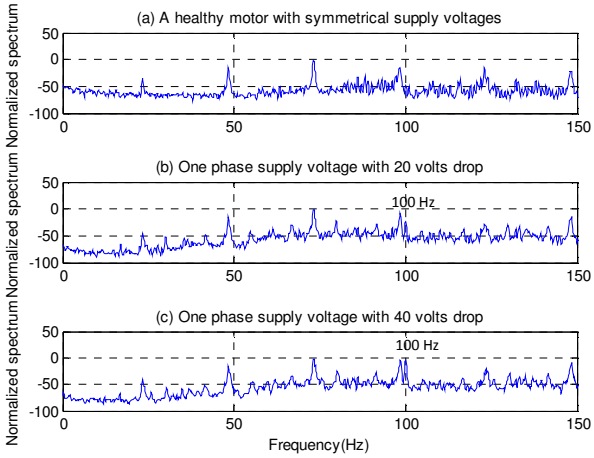

Figure 11 The vibration power spectra of induction motor without and with 20V and 40V drop of one phase voltage

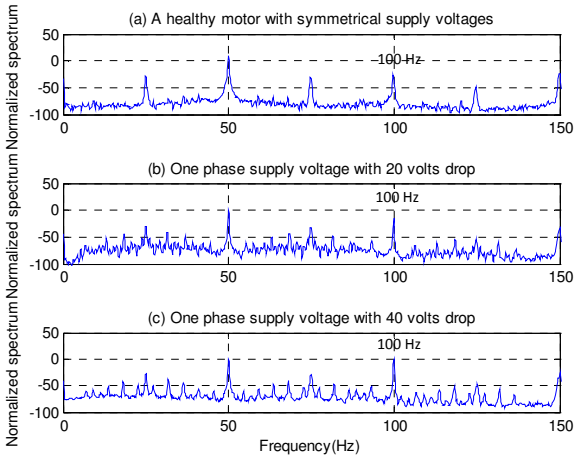

Figure 12 The stator current power spectra of induction motor without and with 20V and 40V drop of one phase voltage

From figure 5-7 (b), figure 8-10 (b) and figure 11 (b)-(c), it is noticeable that the plenty of harmonics and sidebands appear in the vibration and stator current spectra of a faulty induction motor. On one hand it provides us some extra information about the induction motor condition, however, on the other hand it does add some extra load for us to sort out what those harmonics and sidebands frequencies are and how they are related to each other. Cepstrum Analysis is especially useful for detecting these harmonics and sidebands. As while a frequency spectrum or FFT reveals the periodicity of a time domain measurement signal, the cepstrum reveals the periodicity of a spectrum. Figure 13 presents the cepstrum of an induction motor vibration without and with one broken rotor bar. It is can be seen that the cepstrum of the motor without broken rotor bar fault only shows the fundamental rotating quefrecy 40.8 ms (equal to motor speed 24.5 Hz) and its quefency harmonics 20.4 ms (equal to 2 times motor speed 49 Hz). However for an induction motor with broken rotor bar fault the cepstrum gives some extra information about the sidebands associated with broken rotor bar fault. For example, in figure 13 the clear quefrecy components at 285.7 ms and 142.8 ms which equals to 3.5 Hz and its harmonic 2×3.5 Hz separately. The 3.5 Hz is the twice slip frequency of the induction motor. As it is stated before, the general basis for induction motor fault detection is that a fault in the motor circuit causes an asymmetry in the flux density across the motor circuit and this flux imbalance rotates with the rotor. The effect of this rotating electrical imbalance can be detected both in stator vibration, consumed current and transient rotor speed, and in each case it appears as a modulation effect with a modulating frequency of twice slip. The 3.5 Hz is deduced as follows: 2×slip=2×(1500rpm-1447rpm)÷1500rpm×50Hz=3.5 Hz

When compared with the power spectrum analysis in figure 5, the cepstrum in Figure 13 demonstrates some advantages like more simple and concise characteristics. The similar phenomenon can be observed in figure 14 for induction motor current cepstrum without and with one broken rotor bar. The quefrecy components 142.5ms

and 285ms are noticeable. These results prove that cepstrum analysis is a very useful tool for detection families of harmonics with uniform spacing or the families of sidebands. It compresses the complicated families of harmonic and sidebands frequencies shown in power spectrum into concise and simple quefrecy components which can be easily identified and evaluated.

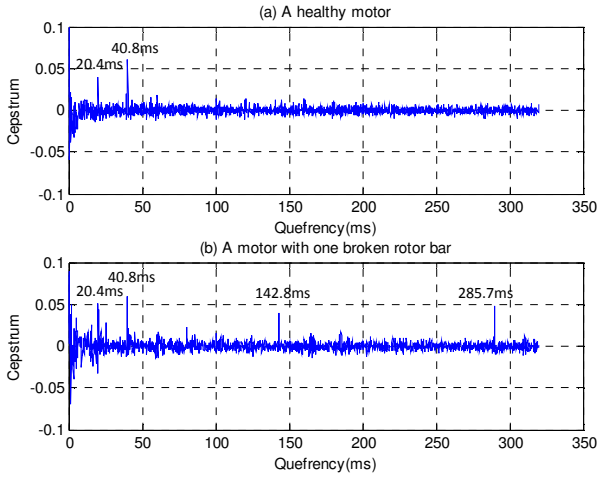

Figure 13 The vibration cepstrum of induction motor without and with broken rotor bar fault

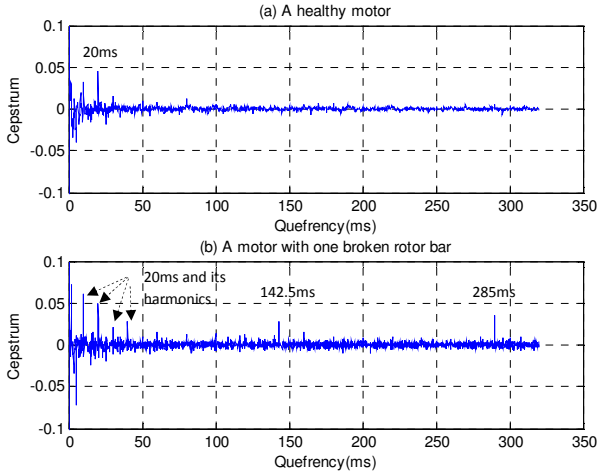

Figure 14 The stator current cepstrum of induction motor without and with broken rotor bar fault

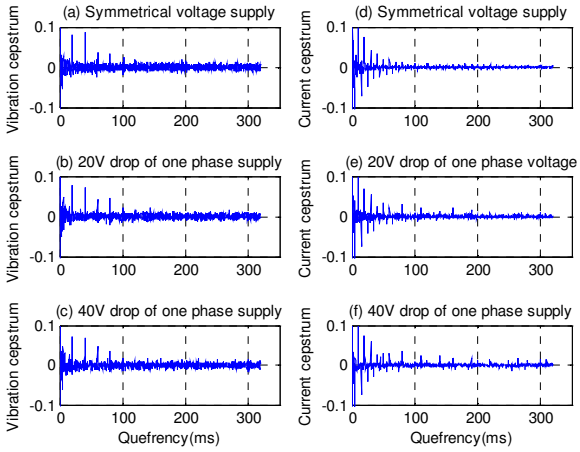

Figure 15 The vibration and stator current cepstrum of induction motor with 20V and 40V drop of one phase voltage

Figure 15 presents some results of vibration cepstra (figure 15 (a)-(c)) and current cepstra (figure 15 (d)-(f)) for an induction motor under symmetrical voltage supply, 20V and 40V drop of one phase voltage situations. It is found that both vibration and current cepstra show very similar except that some small differences of quefrency components exist between 100ms to 300ms in the stator current cepstra. Due to the fact that the main symptom for unsymmetrical voltage supply is $2\times\omega$=100 Hz which is not a series of periodic components in the power spectrum, the cepstrum results do not show any particular advantages to identify this kind of fault.

Figure 16 shows a vibration bispectrum of a healthy induction motor. It can be seen that only two significant peaks appear around [300Hz, 550Hz] and [550Hz, 300Hz], and two minor peaks at [300Hz, 850Hz] and [850Hz, 300 HZ], which suggesting the coupling between these frequencies. These frequencies are less interested for us because they are associated with the electromagnetic supply frequencies of the induction motor. This assumption can be identified by the linear power spectra comparison in figure 17, which clearly shows the peaks at 300Hz and 850Hz in induction motor vibration. Figure 18 presents one of vibration bispectrum of a motor with one broken rotor bar. The figure indicates much richer component bispectrum coupling than the bispectrum in the healthy motor. But the expected rich sidebands cross talking and modulation have not been observed, which are supposed caused by the very low amplitude of the sidebands. If a comparison is made between Figure 16 and 18, it can be seen that there are the clear patterns of bispectra in vibration for a healthy and faulty motor.

Figures 19-20 show the bispectra for the seeded unsymmetrical voltage supply faults (20v and 40v drops in one phase of power supply). It can be seen when the unsymmetrical stator voltage increases, the bispectrum peaks shift and concentrate around 100 Hz (the typical fault symptom for an asymmetrical stator fault) [15]. Additionally other irrelevant components are suppressed. The 100 Hz component and its harmonic 200 Hz component increase while the 300 Hz component decreases significantly when the extent of asymmetry in the per-phase voltage increases. But the amplitudes of 100 and 200 Hz components show relatively less rises in the power spectrum when compared with the bispectrum. The similar things can also be observed from the stator current bispectra. Figure 21 presents the stator current bispectra of a motor in normal and one broken rotor bar conditions. In order to compress the dominate 50 Hz power supply frequency component, the logarithm bispectrum is adopted. It can be seen that there are of rich sidebands components in stator current bispectrum associated with one broken rotor bar motor (figure 21-(c)). For 20v and 40v drops in one phase of power supply, the stator current bispectrum (figure 22) also show some similar characteristics like what happened in vibration bispectrum. The faulty symptom 100 Hz is the major frequency component. Therefore these results demonstrates that bispectrum analysis in comparison with conventional power spectrum analysis is particularly useful in suppressing some irrelevant components and highlighting the components of interest.

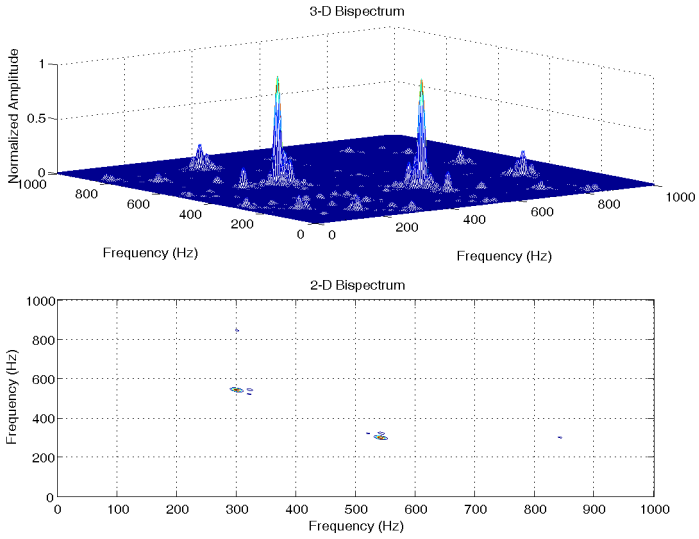

Figure 16 The vibration bispectrum of a healthy motor

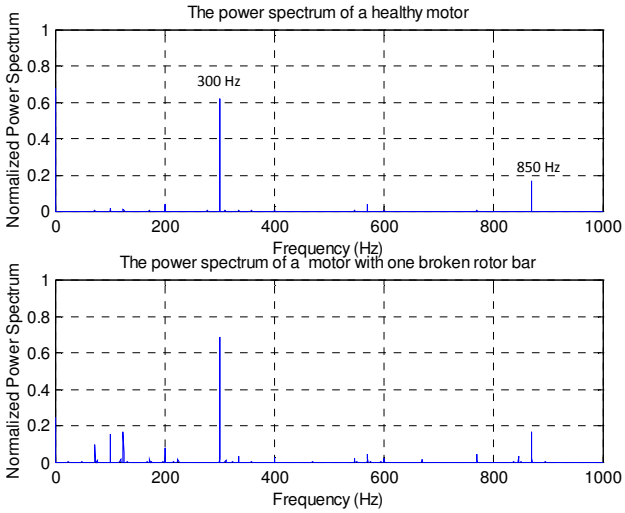

Figure 17 The linear vibration power spectra for a motor without and with one broken rotor bar

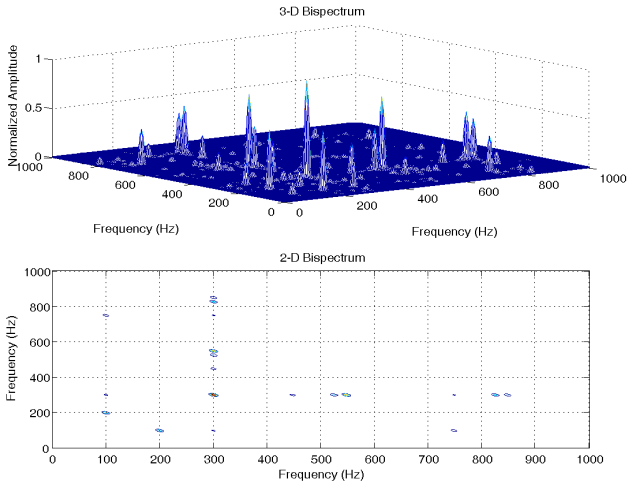

Figure 18 The vibration bispectrum of a motor with one broken rotor bar in vibration

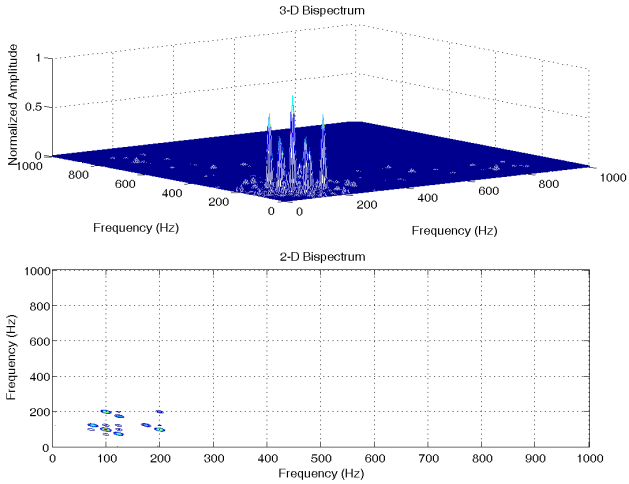

Figure 19 The vibration bispectrum of a motor with a 20v drop in one phase of supply

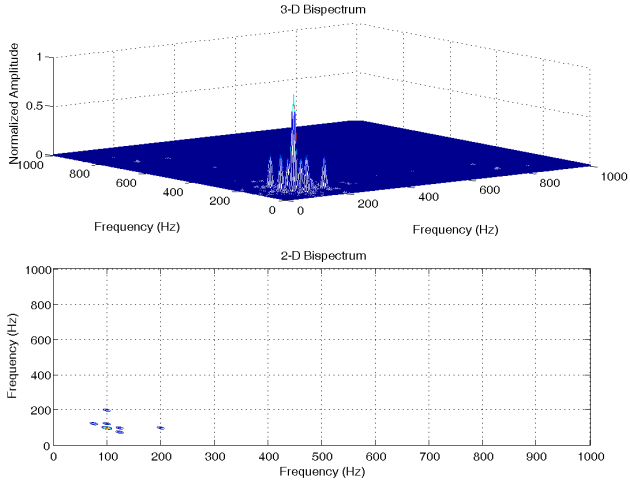

Figure 20 The vibration bispectrum of a motor with a 40v drop in one phase of supply

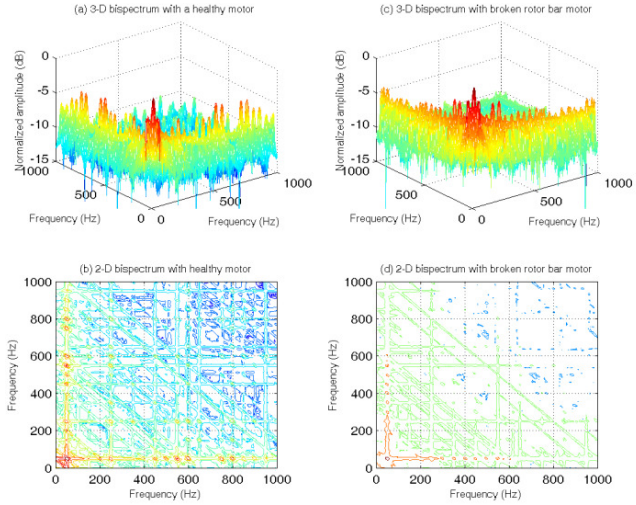

Figure 21 The stator current logarithm bispectra of a motor without and with one broken rotor bar

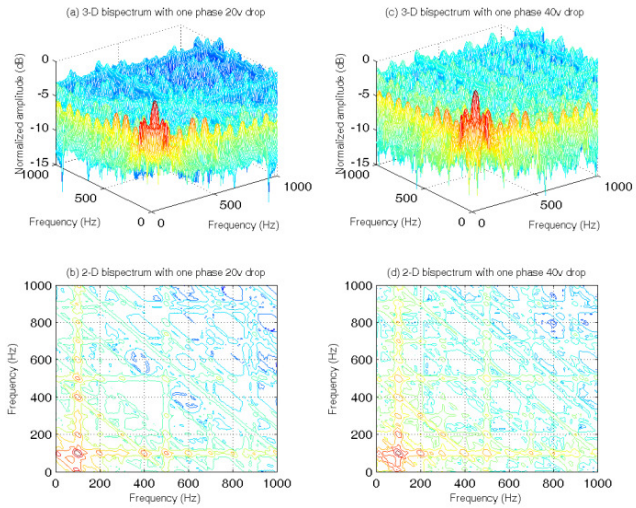

Figure 22 The stator current logarithm bispectra of a motor with a 20v and 40v drop in one phase of supply

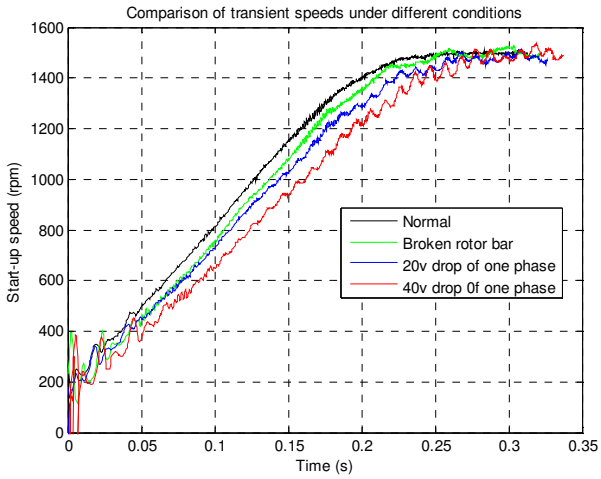

Figure 23 The comparison of starting transient speeds under different conditions

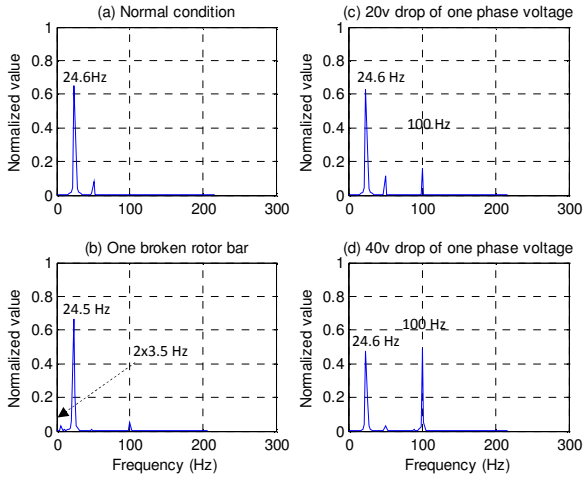

Figure 24 Spectra of starting transient speeds under different conditions

Due to the resultant no-zero negative sequence component of mmfs and the unwanted pulsing torque caused by faults in induction motor, the instantaneous angular speed of induction motor will be changed as well. Therefore a series of instantaneous angular speed measurements for the induction motor start-up were made. Figure 23 gives the transient speeds of the induction motor during its start-up under different situations. The transient speeds show clearly speed ripples for 20v and 40v unsymmetrical voltage power supply. The amplitude of speed ripples increases with the rising of unsymmetrical voltage power supply. The power spectra of the transient speeds are presented in figure 24. All relevant symptoms for corresponding faults are identifiable, for example, the two times sideband modulation frequency about 7 Hz for one broken rotor bar fault, the 100 Hz ripple frequency for 20v and 40v unsymmetrical voltage supply faults. The transient speed variations of induction motor start-up exhibit good sensitivity for a faulty induction motor as the induction motor speed is governed by the electrical torque which is influenced by the stator and rotor conditions of the induction motor. No cepstrum and higher order spectrum analyse were carried out for transient speed of the induction motor as its frequency components are few.

Finally a backpropagation neural network was applied to do the job for automatic fault detection. The parameters selected include the most directly parameters to the fault symptoms of induction motor. Time domain signals were not employed as inputs to backpropagation neural network, rather the frequency spectra. In order to reduce the neural network inputs, cepstrum and bispectrum of vibration and stator current were not used. As it was indicated in section 3, the asymmetrical stator phase voltage will have big 100 Hz symptom component in its vibration or transient speed spectra. Damage to the rotor bars is characterised by the existence and growth of sidebands around the rotating speed of shaft. One method involves observing the magnitude of the power spectrum over the rotor rotation frequency both up and down in vibration spectrum, and the main supply frequency 50 Hz in the stator current spectrum. In the summery, the following frequencies were adopted to be inputs for the neural network:

(a) The means, variance, skewness and kurtosis of vibration and current in time domain (eight inputs)
(a) The amplitudes of current power spectra at the sidebands: $(1\pm n\times 2s)\omega$, n=1,2,3. (six inputs).
(b) The amplitude of vibration power spectra at the sidebands $(1\pm n\times 2s)\omega_r$, n=1,2,3 (six inputs).
(c) The average of amplitudes of the first three upper and lower sidebands surrounding the rotor speed frequency and its second and third harmonics in the vibration spectrum (three inputs).
(d) The average of amplitudes of the first three upper and lower sidebands surrounding the main supply frequency in current power spectrum (three inputs).
(e) The amplitudes of 100 Hz, 200 Hz and 300 Hz in vibration spectrum and 100 Hz in transient speed spectrum (four inputs).

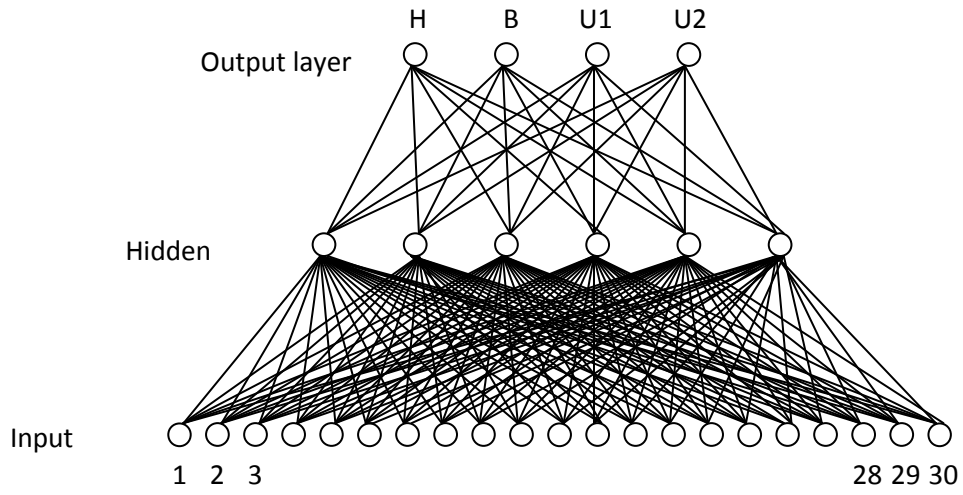

Figure 25 The structure of neural network with parameter set one

The neural network with parameter set one contained a total of 30 inputs nodes, six hidden nodes and four output nodes corresponding to normal, broken rotor bar, phase unbalance one and phase unbalance two. The Figure 7.3 shows the structure of the neural network. The letter H, B, U1 and U2 separately stand for health, Broken rotor bar, unbalance 20v of phase voltage and unbalance 40v of phase voltage. The number of nodes in the hidden layer has been obtained by trial and error. The results are summarised in Table 2. Because a network with less than 3-4 nodes in the hidden layer could hardly converge to the desired error, the table doesn't give the results with less than five hidden nodes. From the table 2 it can be seen the more nodes used means the longer training time is needed to reach the error target. Also the generalised characteristic of a neural network will become poor with higher hidden nodes because the likelihood of training success will decrease.

Table 2 The hidden node effects

	Training time (s)	Learning rate
5 hidden nodes	<20	0.01
6 hidden nodes	<30	0.01
7 hidden nodes	<50	0.01
8 hidden nodes	<120	0.01

A total of 500 test sets were conducted using the above backpropagation model. 300 of these data sets were used to train the neural network. They are: 150 tests involved an entirely undamaged motor, and were used to established the baseline and provide data for normal condition readings; 50 test sets involving one broken rotor bar were conducted; 50 test sets were performed for 20v drop of one phase voltage; and 50 test sets were performed for 40v drop of one phase voltage. The remaining 200 test sets were divided into 100 sets for testing and 100 sets for validating the output neural network (each 100 sets including 25 sets for normal, 25 sets for broken one rotor bar, 25 sets each for 20v drop and 40v drop of one phase voltage).

The procedures are: (1) In the pre-processing phase, the input values are normalized in the range of [-1,1]. (2) During training stage, the neuron's weight and bias values are adjusted by the steepest descent algorithm. (3) Finally the mean squared error (MSE) is used as a metric for measuring the neural network's performance.

$$\mathrm{MSE} = \frac{1}{N}\sum_{i=1}^{N}(O_i - T_i)^2 \tag{16}$$

Where O_i is the ith neuron's output, T_i is the designated value for the ith output neuron, N is the total output neurons.

Some test results are shown in Table 3. It can be seen that the average MSE errors for the testing and validating sets show good agreement despite the validating MSE error seems slightly higher than the testing MSE error. This kind of error may be caused by few samples and the randomness of samples.

Table 3 Neural network performance

Normal (Average MSE error for all 25 samples)		Broken rotor bar (Average MSE error for all 25 samples)		Unbalance(20v) (Average MSE error for all 25 samples)		Unbalance(40v) (Average MSE error for all 25 samples)	
Testing	Validating	Testing	Validating	Testing	Validating	Testing	Validating
0.0113	0.0182	0.0162	0.0207	0.0272	0.0288	0.0213	0.0232

4. CONCLUSIONS

This paper compares the effectiveness of some signal processing techniques for vibration, phase current and transient speed analyses for detection and diagnostics of induction motor faults, on the basis of experimental results. In particular, the capability of approaches based on power spectrum, cepstrum and bispectrum (one of higher order spectra) analysis are compared each other. For each technique, the sensitivity to a few common faults in induction motors like broken rotor bars, unsymmetrical stator voltages caused by stator shoutcuts are assessed. It has found that for vibration signal, power spectrum, cepstrum and bispectrum present better ability to identify induction motor faults if the fault symptoms demonstrate characteristics in rich sidebands and harmonics. In particular applying cepstrum in the vibration signal of induction motors can make a complex power spectrum looking much more concise and simpler. However if the fault symptoms show a single frequency line and demonstrate no harmonic frequencies, applying cepstrum either in the vibration signal or stator current signal of induction motors will show less advantage. It has been found that clear and different bispectrum patterns exist between healthy and faulty conditions of induction motors. One of biggest advantages of the bispectrum analysis is its ability to suppress Gaussian noise and provide some extra phase coupling information in signals. Traditional power spectrum analysis possesses neither of these properties. The bispectrum therefore can provide us an effective means for fault feature extraction and recognition. A simple backpropagation neural network was used and the satisfactory detection probability was obtained. A combination of all three techniques plus neural network should undoubtedly provide us a better tool for condition monitoring and fault diagnosis of induction motors.

REFERENCES

[1] L.Cohen, "Time-Frequency Analysis: theory and application", Prentice Hall Signal Processing Series, 2003

[2] J.M. Mendel, "Tutorial on higher order statistics (spectra) in signal processing and system theory: theoretical results and some application", Proceedings of the IEEE, Vol.79 March 1991, pp.278-305

[3] G. Fengshou and A. Ball, "Electrical motor current signal analysis using modified bispectrum for fault diagnosis of reciprocating compressors", Proceedings of COMMADEM 2009, Sweden

[4] G. Fengshou, etc "Electrical motor current signal analysis using modified bispectrum for fault diagnosis of downstream mechanical equipment", Mechanical System and Signal Processing, Vol 25 (1), 2011, pp360-372

[5] R.B.Randall, "Cepstrum analysis and gearbox fault diagnosis", Application Notes, Brüel & Kjær, 1989

[6] M.Aladesaye, "Application of predictive theory and application", A PhD thesis, Massey University, France, 2008

[7] D.R. Brillinger, "An introduction to polyspectra," *Ann. Math. Stat*., Vol. 36, 1965

[8] C.L. Nikias, and A.P. Petropulu, "Higher order spectral analysis: A Nonlinear Signal Processing Framework" Prentice-Hall Inc. 1993
[9] D.R. Brillinger, "Some basic aspects and uses of higher order spectra", Signal Processing, Vol.36, 1994, pp.239-249
[10] A.P. Petropulu, "High-order spectral analysis", CRC Press LLC, 2000
[11] B. Adkins, "The general theory of electrical machines", Chapman & Hall Ltd., London 1957
[12] W.A.F. Justin, "Bispectral analysis of speech signals", Ph.D. thesis, The University of Edinburgh, 1996
[13] B. Liang, "Condition monitoring and fault diagnosis of electrical machines", Ph.D. thesis, The University of Manchester, 2000
[14] G.B. Kliman, R.A. Kogel, J. Stein, R.D. Endicott and M.W. Madden, "Non-invasive detection of broken bars in operating induction motors". IEEE Transactions on Energy Conversion, Vol.3, No.4, 1998, pp.873-879
[15] V.A. Kinitsky, N. Rotondale, M. Martelli, and C. Tassoni, "Harmonic analysis of induction motors with stator faults". Electrical Machines and Power Systems, Vol.22, Pt.B, 1994, pp.215-231
[16] P.Vas, "Parameter estimation, condition monitoring and diagnosis of electrical machines", Oxford science publications, 1989